Orientation Gradients at Polymer Surfaces. I. Description of Methods

GANGCHI CHEN and LESLIE J. FINA*

Rutgers University, Department of Materials Science and Engineering, College of Engineering, P.O. Box 909, Piscataway, New Jersey 08855-0909

SYNOPSIS

A method capable of quantitative predictions of orientation gradients at the surface of polymers is proposed. It is based on the transformation of variable-angle attenuated total reflected infrared intensities to absorption coefficients versus depth from the surface. Two alternate approaches have been used to demonstrate the viability of the method: computer simulation and sample analysis. Exact reflected intensities from anisotropic layered systems have been calculated with Fresnel coefficients. The exact intensities are used to reextract the orientation gradient with data transformation. This analysis demonstrates the conditions under which the variable-angle method is expected to optimally perform. Simulation results clearly indicate high accuracy near the interface and low accuracy at remote distances. Thin films of isotropic and uniaxially drawn isotactic polypropylene are prepared and used as layered systems. Step functions in orientation can be accurately predicted only when some information is known prior to the gradient calculation. In uniaxially oriented thick films of polypropylene, the analysis indicates that the crystal phase is highly oriented at the surface and in the bulk. Within the first 2 microns from the surface, both the amorphous and crystal phases show negligibly small gradients in orientation. © 1993 John Wiley & Sons, Inc.

INTRODUCTION

A number of analytical methods have been recently applied to polymer surfaces that can provide compositional or structural information as a function of depth from a surface. Tingey and Andrade[1] and Gardella[2] summarized commonly used methodologies. Often, multiple methods are used to probe the same samples since each is sensitive to a different range of depths from the surface. Whereas contact angle measurements, ion scattering spectroscopy, and secondary ion mass spectroscopy are extremely surface-sensitive (0–10 Å), infrared spectroscopy is on the other end of the depth spectrum, probing distances from 0 to 2 microns. A few of the surface-sensitive methods can provide depth profiling information by the variation of an experimental parameter, e.g., the electron takeoff angle in X-ray photoelectron spectroscopy (XPS)[3,4] and the angle of incident light in attenuated total reflection (ATR) fluorescence.[5] Both XPS and ATR spectroscopies provide composite depth information when the takeoff or incident angle is varied. Recently, Dittmar et al.[6] approached the depth resolution of composite information with the use of photoacoustic infrared spectroscopy in combination with step-scan interferometry. A depth resolution of about 0.8 micron is based on a constant infrared modulation frequency in combination with a phase resolution of the outgoing acoustic signal. Miller and Bohn[7] explored the use of wave guide Raman scattering in a model analysis to determine dopant distributions in polystyrene thin films. It was concluded that any available information known beforehand about the functional form of the profile is a valuable aide to the problem.

Depth profiling with the use of ATR infrared reflection spectroscopy has been accomplished by a variation in the depth of penetration. This can also be described as a variation in the rate of decay of the evanescent wave that propagates from the re-

* To whom correspondence should be addressed.

Journal of Applied Polymer Science, Vol. 48, 1229–1240 (1993)
 CCC 0021-8995/93/071229-12

flection crystal element into the sample medium. The depth of penetration is experimentally varied by a change in the refractive index of the reflection element or in the angle of incident light. Many studies have been done that exploit this property to probe chemical and structural differences between the surface and the bulk. Urban and Koenig reviewed the area.[8] Popli and Dwivedi[9] used a combination of incident angular variation and two internal reflection crystals to show nonhomogeneous distributions in solvent-cast polymer blends. Zerbi et al.[10] probed the surface of polyethylene with variable-angle ATR and predicted the distribution of crystallinity from the surface. Studies such as these can be considered semiquantitative since the depth of penetration is a measure of the evanescent wave decay. To obtain quantitative distribution information, the ATR intensities must be inverse Laplace transformed, as has been described elsewhere.[11-15]

Depth profiling of orientation at polymer surfaces has been approached semiquantitatively by a limited number of researchers.[16-18] Tshmel et al.[16] compared the bulk and average surface orientation in several uniaxially drawn polymers with infrared transmission and ATR modes, respectively. A generally observed phenomenon is a surface that is more highly oriented than is the bulk. Contrarily, Hobbs et al.[17] observed a negligibly small orientation gradient in uniaxially drawn polypropylene. The goal of this work is to explore and extend the variable-angle ATR methodology originally proposed by Hirschfeld[19] to include a quantitative prediction of the orientation distribution as a function of distance from a polymer surface. In some cases, the distributions cannot be correctly predicted, particularly when there is no *a priori* knowledge of the form. Nonetheless, under conditions described in this work, a considerable improvement in quantitative orientation gradient analysis can be realized.

EXPERIMENTAL

Sample Preparation

Thin isotropic and uniaxially oriented films of isotactic polypropylene (obtained from American Renolit Corp.) were prepared in the following way: The isotactic polypropylene was ground to a powder in liquid nitrogen. The powder was placed between aluminum foil sheets and heated in a press to 180°C. The samples were next quenched in iced water and then uniaxially stretched at room temperature. This treatment resulted in 4–7 microns isotropic films and 1–2 microns oriented films. Thicker isotropic and uniaxially oriented films were prepared from the melt-quenched 130 microns-thick original commercial isotactic polypropylene film.

Spectroscopy

The FTIR–ATR data collection was carried out with a resolution of 2 cm^{-1} and 200 scans on a Perkin-Elmer 1750 model Fourier transform infrared spectrometer equipped with an MCT detector. A single reflection accessory (Specac 19653) was used with a zinc selenide hemispherical crystal to facilitate variable-angle collection. A special ATR sample holder was designed to optimize optical contact. In all experiments, a constant torque of 10 in.-pounds was used to maintain constant sample–crystal contact. The optic axis of the polymer was placed coincident with the *s*-polarized light direction. In all variable-angle studies, a 1 mm-diameter beam aperture was used to increase the accuracy of the incident angle and eliminate polarization mixing. Incident light was polarized by a commercially manufactured gold wire grid polarizer with a AgBr substrate (Perkin-Elmer 0186-243). All spectra were sent to a DEC VAX Cluster for data processing and analysis.

RESULTS AND DISCUSSION

Simulation Studies

The prediction of reflected and transmitted intensities from a layered system of thin films of arbitrary variation in optical constant anisotropy is a formidable problem. Treatments have been proposed that involve the calculation of an interference matrix that relates electric-field amplitudes at the initial and final boundaries of the layered system.[20-22] The transmitted and reflected intensities are found from the elements of the interference matrix. Inaccuracies in the calculations occur when products or sums of elements approach zero. To avoid these problems, the equivalence of the electric-field strength in the transmission and ATR modes is used as the basis for the calculation of reflected intensities. This treatment is given in some detail elsewhere.[11,13] The starting point for the use of the equivalence to probe oriented systems is a modified form of the Laplace equation, i.e.,

$$1 - R(\theta) = \frac{4\pi\langle E_{02}^2\rangle}{n_1\lambda\cos\theta} \times \int_0^\infty n_2(z)k_2(z)\exp \times\left(-\frac{z}{d_p(\theta)}\right)dz \quad (1)$$

where R is the experimental attenuated totally reflected intensity as a function of incident angle θ; $\langle E_{02}^2 \rangle$, the electric-field strength at the surface of the probed material; n_1, the refractive index of the incident medium; λ, the wavelength of incident light; n_2, the refractive index of the probed medium as a function of depth z; k_2, the absorption coefficient of the probed medium; and d_p, the depth of penetration of the evanescent wave. Equation (1) is modified from previous treatments by the inclusion of n_2 under the integral. Normalization of the left side of eq. (1) by the preintegral term on the right leads to information about the form of the optical constant gradient without solving the integral.[11]

Anisotropies in the optical constants, n_2 and k_2, and in the surface electric-field strength exist for oriented systems. Additionally, for systems with orientation gradients, the optical constants are depth-dependent. Equation (1) cannot be solved for these unknowns given the experimental reflected intensities. However, modeling studies are informative in terms of their use to probe polymer systems. Of primary interest is the anisotropy and gradient in the absorption coefficient k_2. The exact reflected intensities for a two-phase system can be found from the following relationships[23]:

$$\tilde{\rho}_s = \frac{(\tilde{n}_x^2 - n_1^2\sin^2\theta)^{1/2} - n_1\cos\theta}{(\tilde{n}_x^2 - n_1^2\sin^2\theta)^{1/2} + n_1\cos\theta} \quad (2)$$

$$\tilde{\rho}_p = \frac{n_1(\tilde{n}_z^2 - n_1^2\sin^2\theta)^{1/2} - \tilde{n}_y\tilde{n}_z\cos\theta}{n_1(\tilde{n}_z^2 - n_1^2\sin^2\theta)^{1/2} + \tilde{n}_y\tilde{n}_z\cos\theta} \quad (3)$$

$$R = \tilde{\rho}\tilde{\rho}^* \quad (4)$$

where the x direction corresponds to the s-polarized direction and z is perpendicular to the interface. $\tilde{n}_i$ is defined in this work as $n_i - ik_i$. Modifications of eqs. (2)-(4) allow for its use with a three-phase system. Figure 1 shows the calculated reflectances for a two-phase system using optical constants that are typical of polymers. Curves A and B are calculated using the same absorption coefficients and a refractive index (n) change of 0.07 units. This level of n variation can be considered as an average amount of birefringence for oriented polymers. These curves illustrate that the refractive index anisotropy can be ignored at large angles of incidence for a k value of 0.01. However, a close approach to the critical angle of internal reflection (38.3°) is required to provide the Laplace eq. (1) with a sufficient variation in the depth of penetration.[19] Curves C and D of Figure 1 show the same comparison at a larger absorption coefficient value (0.10). In this case, the refractive index anisotropic of oriented polymers cannot be neglected except at incident angles approaching 90°. Therefore, in general, the refractive index anisotropy cannot be ignored in the calculation of orientation gradients.

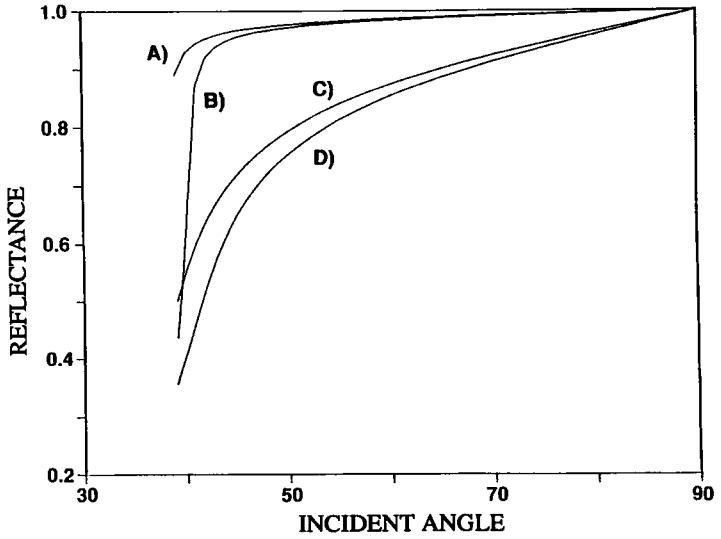

Figure 1 Exact attenuated total s-polarized reflectances calculated with eqs. (2)-(4) for a two-phase system where the incident phase is isotropic and nonabsorbing ($n_1 = 2.42$) and the final phase is absorbing. (A) $k_x = 0.01$, $n_x = 1.50$; (B) $k_x = 0.01$, $n_x = 1.57$; (C) $k_x = 0.10$, $n_x = 1.50$; (D) $k_x = 0.10$, $n_x = 1.57$. (Reprinted with permission from the *Advances in Chemistry Series* in *Structure-Property Relations in Polymers: Spectroscopy and Performance*, C. Claver and M. Urban, eds., Copyright 1992, American Chemical Society.)

Also of primary concern in the calculation of orientation gradients at surfaces is the refractive index gradient that accompanies an absorption coefficient gradient. A determination of the relative importance of these gradient types is instructive for the use of eq. (1). Figure 2 shows the calculated *s*-polarized reflectances from eq. (1) that has been used in a form where n_2 and k_2 depend discretely on depth z rather than continuously.[13] The top curve is the reflectance for a system with gradients in both n_2 and k_2 (k_2 linearly decreases from 0.02 at the surface to 0.01 at 0.6 micron and is constant thereafter; n_2 linearly decreases from 1.50 at the surface to 1.40 at 0.6 micron and is constant thereafter). A comparison of this curve that takes into account gradients in both optical constants with the remaining three yields information about the relative importance of individual optical constant gradients. The bottom two dashed curves are calculated with no gradients in k_2 [$k_2(z) = 0.02$ for all z]. Clearly, neglecting the gradient in k_2 significantly alters the reflectance calculation. Conversely, neglecting the gradient in n_2 and retaining the gradient in k_2, as shown in the dotted curve [where $n_2(z) = 1.50$ for all z], does not significantly alter the calculated intensities from the top curve. Figure 2 is interpreted to mean that the refractive index gradient can be neglected when eq. (1) is used to probe experimental systems. This is particularly true in polymers with small $P_2(\cos\theta)$ values or large $P_2(\cos\theta)$ values accompanied by small birefringence values. An example of the latter is polypropylene.

Up to this point, the reflected intensities have been calculated directly from the optical constants. In an experiment, the intensities are measured and used in eq. (1) to calculate the gradients. Equation (1) is based on assumptions that limit its accuracy and applicability: They are that (1) $k_2 < 0.10$ and (2) $\langle E_{02}^2 \rangle$ and $d_p(\theta)$ are independent of $k_2(z)$. To a first approximation, the assumptions are met, but, nonetheless, cause inaccuracies in the calculation of the inverse Laplace transform. To define the strengths and limitations of the transform, the exact intensities of model orientation gradients are calculated and used in eq. (1) to solve for the gradient. The model system is shown in Figure 3. n_1 is the refractive index of the nonabsorbing incident phase. $\tilde{n}_i$ are the refractive indices of the absorbing oriented layer. All analyses are done with the optic axis of the probed material as the x-axis or s-polarized direction. The oriented materials are assumed to be uniaxially symmetric. $\tilde{n}_3$ is the refractive index of the substrate.

The first model system treated is homogeneously oriented with the thickness of the layer (d) much greater than the incident wavelength of light (λ).

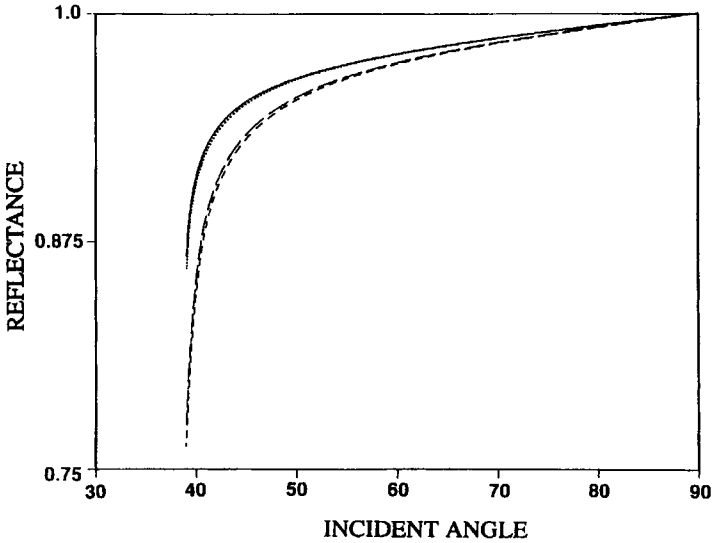

Figure 2 Attenuated total *s*-polarized reflectances calculated with eq. (1) for decreasing linear gradients in the absorption coefficient (k_2) and/or gradients in the refractive index (n_2): (solid line) k_2—gradient, n_2—gradient; (dotted line) k_2—gradient, n_2—no gradient; (large-dashed line) k_2—no gradient, n_2—gradient; (small-dashed line) k_2—no gradient, n_2—no gradient. (Reprinted with permission from the *Advances in Chemistry Series* in *Structure-Property Relations in Polymers: Spectroscopy and Performance*, C. Claver and M. Urban, eds., Copyright 1992, American Chemical Society.)

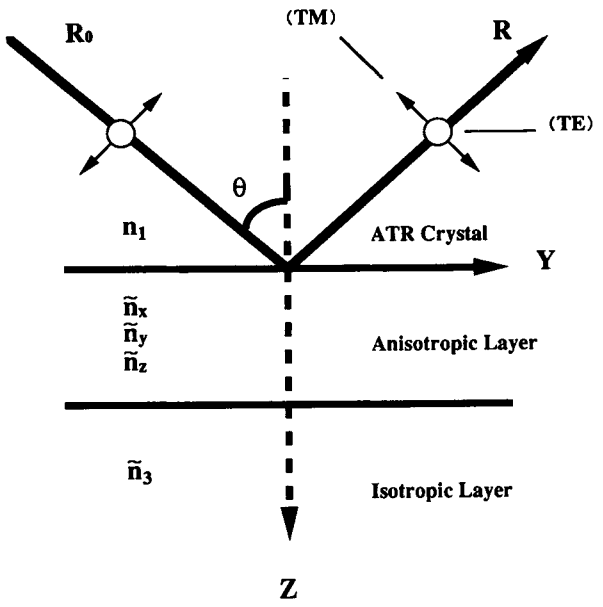

Figure 3 Optical model of a step function in orientation.

Equations (2)–(4) are used to calculate the exact intensities for parallel and perpendicular dipoles. The values for the refractive indicies[24] and absorption coefficients are chosen as those of isotactic polypropylene. The intensities are shown in Figure 4 for dipoles either parallel or perpendicular to the optic axis. The *s*-polarized intensities for parallel dipoles and *p*-polarized for perpendicular dipoles are only shown since remaining intensities are close to 1.0 throughout the angular range. The large drop in intensity near 40° is due to a large increase in the depth of penetration of the radiation. These intensities are used to calculate the gradient with eq. (1). Figure 5 shows the result as the absorption coefficient versus the distance away from the interface. The solid line represents the true solution to the gradient of the homogeneously oriented model system, whereas the dashed lines are calculated solutions using eq. (1). The fitting process does not converge to the true solution. This is a result of the dependence of the depth of penetration and the electric-field intensity on the absorption coefficient that are not taken into account in eq. (1). Figure 5 serves as a general indication of the limitations and accuracy of the methodology for use with orientation gradients. The average error in the calculations at various distances from the interface is shown in Table I. The error is the lowest near the interface, where the electric-field intensity is the strongest, and increases at depths further away.

The second model system treated here is a step function in orientation as modeled in Figure 3. The middle layer is anisotropic and 1.0 micron-thick, while the substrate is isotropic. The optical constants in the calculation of exact intensities are the same as those of Figure 4 for the oriented layer. The isotropic substrate has the constants $n_3 = 1.51$ and $k_3 = 0.00577$. The exact intensities are found with

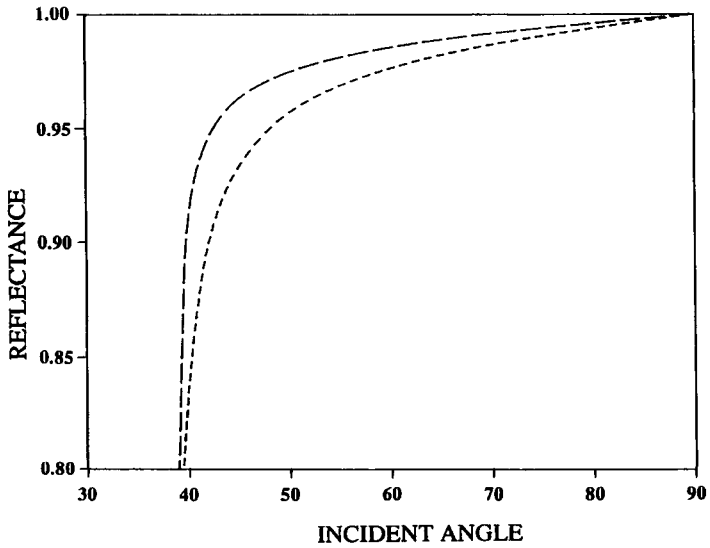

Figure 4 Exact calculated reflected intensities for a homogenously oriented film. $n_1 = 2.42$; $\lambda = 10\ \mu$; $n_x = 1.52$; $n_y = n_z = 1.50$. (Large dashes) dipole parallel to the polymer chain axis, *s*-polarized light, $k_x = 0.01$, $k_y = k_z = 10^{-4}$; (small dashes) dipole perpendicular to the polymer chain axis, *p*-polarized light, $k_x = 10^{-4}$, $k_y = k_z = 0.01$.

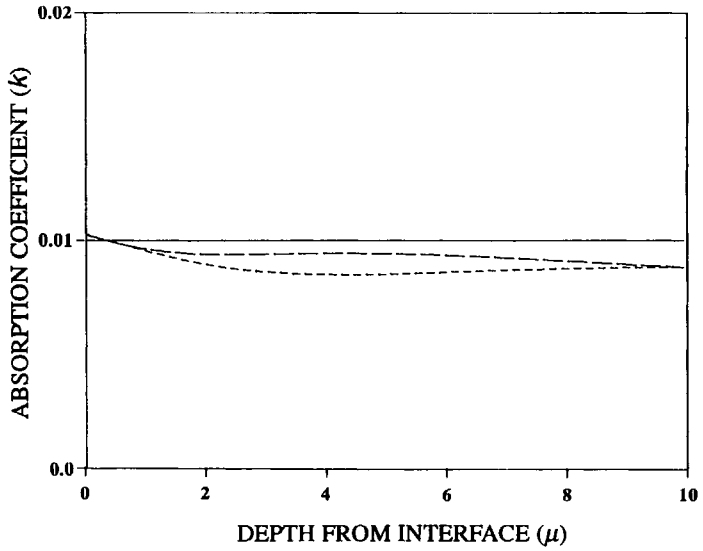

Figure 5 Calculated gradients for a homogeneously oriented system: (solid line) exact solution; (large dashes) calculated solution using *s*-polarized light for dipoles parallel to the polymer chain axis; (small dashes) calculated solution using *p*-polarized light for dipoles perpendicular to the polymer chain axis.

a modified version of eqs. (2)–(4)[23] and have the same general form as those of Figure 4. As in the homogeneous-oriented treatment, the exact intensities are used in eq. (1) to solve for $k(z)$. The calculation procedure is based on a nonlinear least-squares optimization algorithm,[25] which requires input guesses that approximate the actual solution. In Figure 6 is shown the result of the gradient calculation for the orientation step function. The solid lines give the exact (known) solutions. The dashed lines are the solutions calculated with eq. (1) using the exact reflected intensities. The calculated intensities are based on input guesses to the fitting process of $k(z)$ = constant. These guesses led to errors in the solution, suggesting that the algorithm had settled in a local minimum. When a step function in orientation is used as the input guesses to the solution of the inverse Laplace transform, the local minimum is lost, as shown in Figure 7. In this case, the step function gradient is accurately predicted in the first 2 microns and quickly loses accuracy at larger distances. This response is consistent with the exponential decay of the electric-field strength that assumes a value of less than 1% of the surface value at 6 microns for 45° incident light.

Table I Error in Laplace Treatment

Depth (μm)	Error (%)
Interface	2.4
d_p (45°) ≈ 1 μm	3.8
$2 \times d_p$	8.1
$4 \times d_p$	10.2
$8 \times d_p$	10.7
$10 \times d_p$	11.8

Sample Analysis

The variable-angle ATR spectra of a uniaxially oriented thick film of isotactic polypropylene are shown in Figures 8 and 9, *s*-polarized and *p*-polarized, respectively. The polymer chain axis is oriented along the *s*-polarized direction. All peaks show an intensity decrease as the incident light angle increases, which is a combined function of the depth of penetration and the surface electric-field strength. The slight derivative shape to the peaks in Figure 8 at the lowest incident angle is due to an approach to the critical angle of internal reflection [$\sin^{-1}(1.52/2.42) = 38.91°$]. Peaks that are analyzed in this study are indicated in Figures 8 and 9 and assignments are given in Table II. The strong absorption of the 973 and 998 cm^{-1} bands in the *s*-polarized spectra and of the 1376 cm^{-1} band in the *p*-polarized spectra is an indication of the large degree of orientation.

Optical contact is of critical importance in quantitative ATR work. As pointed out by several authors,[16,32,33] the $\ln(R_{Tm})/\ln(R_{Te})$ ratio is a sensitive measure of optical contact. At an incident angle of

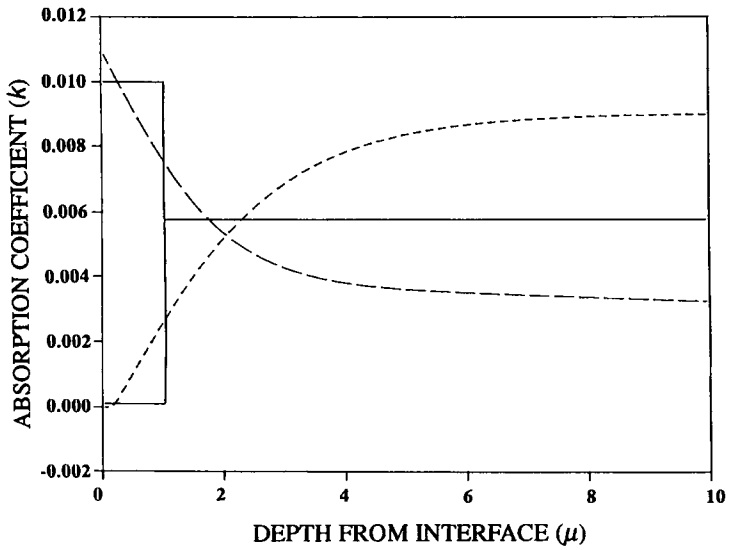

Figure 6 Depth profiling gradients for a step function in orientation for dipoles parallel to the polymer chain axis. Solid lines are the exact solutions: (upper solid line) s-polarized light; (lower solid line) p-polarized light. Dashed lines are calculated solutions using eq. (1) for $k(z)$ = constant as input guesses: (large dashes) s-polarized light; (small dashes) p-polarized light.

45°, the ratio reduces to 2.0, as can be derived from eqs. (2)-(4). For oriented polymers, the use of this criterion requires the identification of an orientation-insensitive absorption peak. The 1460 cm^{-1} peak has been suggested.[32] Intensities from Figures 8 and 9 yield a ratio of 1.93. Assuming that the 1460 cm^{-1} is completely orientation-insensitive, a high degree of optical contact has been established and a minimum amount of stray or false radiation is present. The intensities of peaks in Figures 8 and 9 have been found from both Lorentzian curve-fitting and pseudobase-line techniques. The intensities are then used to solve a discrete form of eq. (1) for the orientation gradient. As stated previously, the gradient in the refractive index has been neglected. This assumption is valid in isotactic polypropylene where

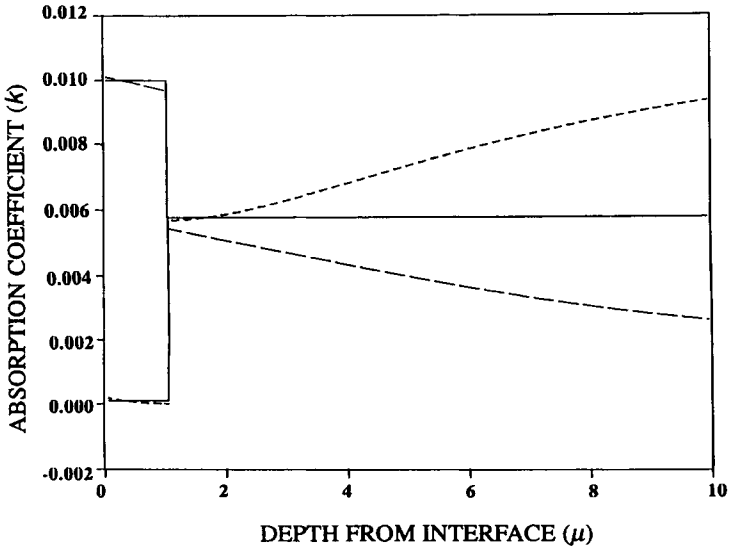

Figure 7 Same as Figure 6 except a step function in the orientation gradients is assumed as input guesses.

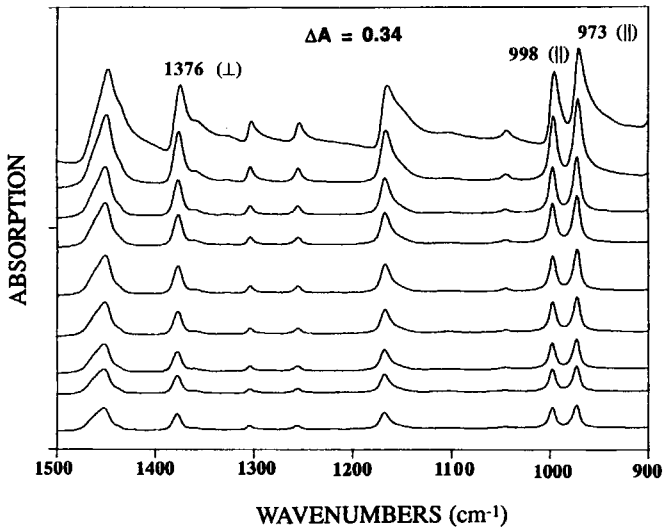

Figure 8 Variable-angle ATR spectra of a thick oriented isotactic polypropylene film (draw ratio = 5.0): *s*-polarized; incident angles from top to bottom: 40, 42, 44, 45, 46, 48, 50, 52, 54.

the birefringence (Δn) for well-oriented samples is 0.02.[24] The refractive index of an isotropic film in the infrared frequency range was found from an interference fringe pattern to be 1.51. Using Δn of 0.02, the refractive index parallel to the chain axis was assumed in the calculations to be 1.52, and perpendicular, 1.50.

The depth-dependent absorption coefficients for the 998 cm^{-1} crystalline peak are shown in Figure 10. The absorption coefficients parallel and perpendicular to the chain axis are included in the figure. Similar results for the 973 cm^{-1} peak are not shown. In the first 2 microns from the interface where the calculation is expected to be the most accurate, very little, if any, depth-dependence is visible. As a test of the accuracy of the Laplace transform in this application, the absorption coefficients have been calculated by independent means. An iteratively fitted Kramers–Kronig transform (KKT) has been applied to an isotropic sample absorption spectrum of isotactic polypropylene. The absorption spectrum is shown at the top of Figure 11, and the calculated

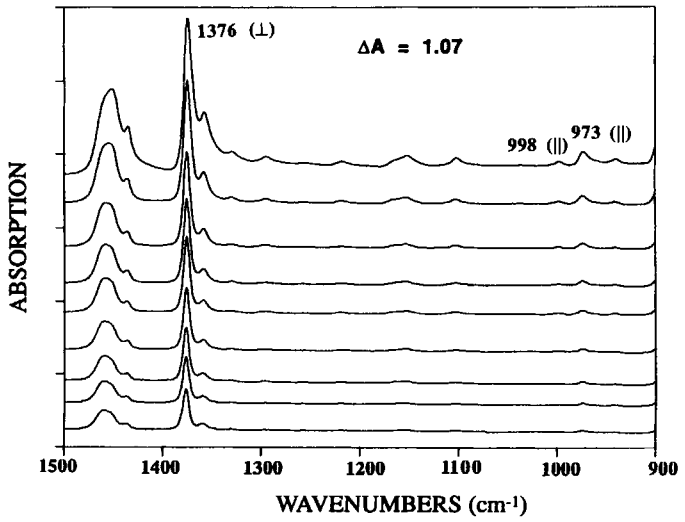

Figure 9 Same as Figure 8 except *p*-polarized incident radiation.

Table II Peak Assignments

Frequency (cm^{-1})	Phase[a]	Polarization	Assignment[a]	Ref.	Transition Moment Angle (Ref. 31)
973	A	∥	$CH_3\gamma$, C—Cν	26, 27	18°
	A, C	∥	$CH_3\gamma$	28	
			$CH_3\gamma$, C—Cν	29	
	A, C	∥		30	
998	C	∥	$CH_3\gamma$, $CH_2\omega$, C$H\delta$	26, 27	18°
	C	∥	Skeletal	28	
			$CH_3\gamma$	29	
	C	∥		30	

[a] A = amorphous; C = crystalline; γ = rock; ν = stretch; ω = wag; δ = bend.

absorption coefficient and refractive index spectra, below. Using the values of the absorption coefficients at the polymer surface in Figure 10 and

$$k_{\text{isotropic}} = \frac{k_{\parallel} + 2k_{\perp}}{3}$$

variable-angle ATR yields k_{iso} for the oriented material of 0.021 for the 998 cm^{-1} peak. This is in close agreement with the KKT prediction of Figure 11, which yields a value of 0.018. It is noteworthy that the k value for the 1376 cm^{-1} peak (0.116) is too large to use either the Flournoy and Schaffers[23] or the Laplace treatment for quantitative results.

The absorption coefficient versus depth curves of Figure 10 can be used directly to calculate a depth-dependent dichroic ratio. However, since the transition moment angles have been determined (Table II), well-known equations to calculate the second moment of the orientation distribution function can be used, i.e.,

$$\langle P_2(\cos\theta)\rangle = \left(\frac{(R-1)}{(R+2)}\right)\left(\frac{(R_0+2)}{(R_0-1)}\right)$$

where R is the dichroic ratio ($A_{\parallel}/A_{\perp}$ or $k_{\parallel}/k_{\perp}$), $R_0 = 2\cot^2\alpha$; α, the angle between the chain axis and the transition moment; and θ, the average angle between the chain axis and the orientation direction. Figure 12 shows the orientation gradients for the

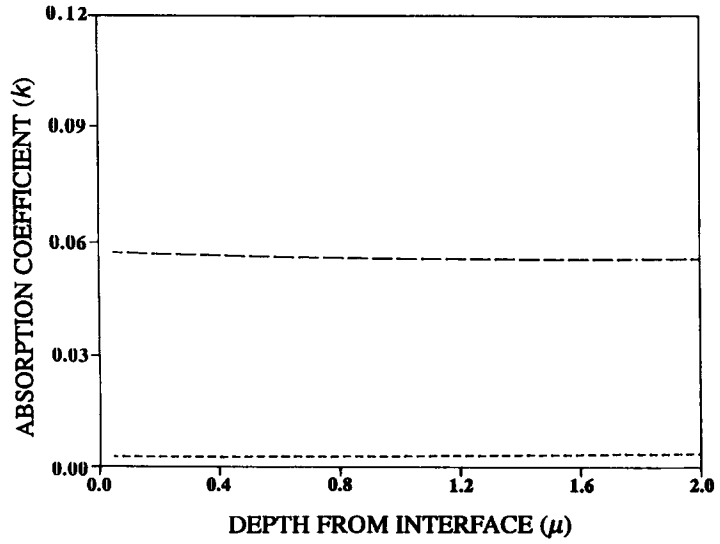

Figure 10 Calculated gradients of 998 cm^{-1} band for homogeneously oriented polypropylene: (large dashes) s-polarized light; (small dashes) p-polarized light.

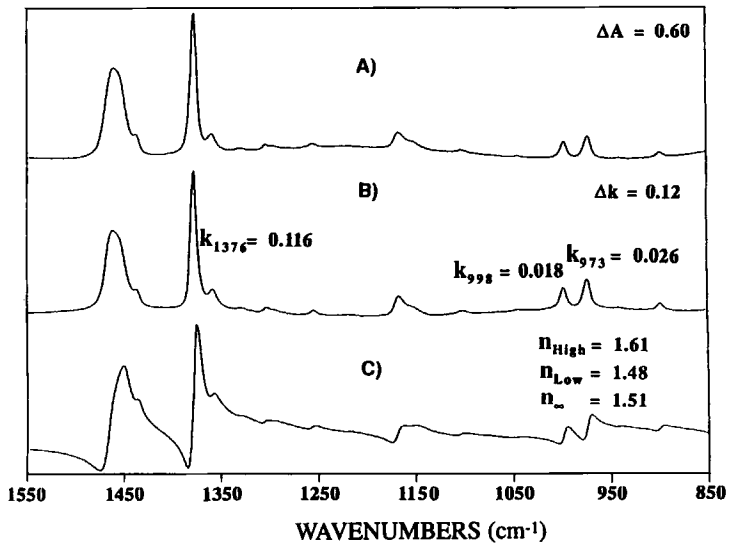

Figure 11 Optical constants of the isotropic polypropylene: (A) absorption spectrum; (B) calculated absorption coefficient spectrum; (C) calculated refractive index spectrum.

first 2 microns from the interface for the 973 cm^{-1} band (crystalline and amorphous contributions) and the 998 cm^{-1} band (exclusively crystalline). The lines represent depth-independent bulk values calculated from dichroic ratios reported in the literature for similarly oriented isotactic polypropylene.[34] The

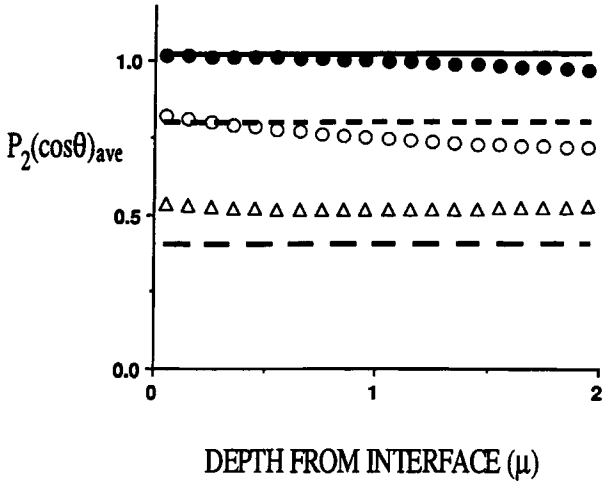

Figure 12 Orientation coefficients vs. depth for uniaxially oriented isotactic polypropylene. Lines are values calculated from bulk dichroic ratios reported in the literature: (solid line) 998 cm^{-1} band; (small-dashed line) 973 cm^{-1} band; (large-dashed line) amorphous phase orientation. Data points are depth-dependent orientation coefficients found from Figure 10. (Closed circles) 998 cm^{-1} band; (open circles) 973 cm^{-1} band; (triangles) amorphous phase orientation calculated from the previous two.

data points are the depth-dependent orientation coefficients calculated from absorption coefficient versus depth curves (e.g., Fig. 10). The top two curves and lines are a result of directly measured intensities, whereas the bottom curve and line are calculated with eq. (5). The relationship between orientation coefficients in the crystal and amorphous phases can be written

$$\langle P_2(\cos\theta)\rangle_{\text{total}} = \chi\langle P_2(\cos\theta)\rangle_{\text{crystal}} + (1-\chi)\langle P_2(\cos\theta)\rangle_{\text{amorphous}} \quad (5)$$

assuming a two-phase system, where χ is the relative amount of crystallinity. The known phase assignment of the 973 and 998 cm^{-1} peaks in polypropylene permit the use of eq. (5) to find the $\langle P_2(\cos\theta)\rangle_{\text{amorphous}}$.[16,31] The value of χ was assumed to be a constant number, 0.64, for the calculation of the bottom line.[34]

The crystallinity is expected to vary with depth, as has been shown previously in polyethylene.[10] The crystallinity gradient is the result of thermal gradients during processing or surface effects that are propagated over relatively large distances. To obtain the crystallinity as a function of depth, we utilize an infrared band ratioing method.[35] Isotropic-equivalent k_{998} and k_{973} values are calculated using the relationship $k_{iso} = [(k_{\parallel} + 2k_{\perp})/3]$ and the experimental data from above (e.g., Fig. 10). Figure 13 shows the k_{998}/k_{973} ratio versus depth from the interface. The absorption coefficient ratio of these two bands is related to the crystallinity through the

density.[35] Figure 14 is the calculated crystallinity versus the depth for the first 2 microns from the interface. Examination of this plot shows that the crystallinity is between 60% and 44% and decreases in the first 2 microns from the interface. Using the depth-dependent crystallinity in eq. (5), the bottom curve in Figure 12 is generated. The apparent orientation gradient reflected in the mixed-phase peak in Figure 12 (circles) translates to a large orientation gradient in the amorphous phase (triangles) if the depth-dependence of the crystallinity is neglected. However, with the consideration of the crystallinity gradient, an orientation gradient is found to be absent in the amorphous phase. This observation is essentially identical to the results of Hobbs et al.[17] However, other published literature reports conclusions that are contrary to ours. We believe that the crystallinity gradient effect accounts for the discrepancy.

Orientation gradient analysis has also been done with layered isotactic polypropylene samples, e.g., a 1.2 micron-thick highly oriented film on an isotropic substrate. The analyses are entirely consistent with the modeling studies presented earlier where the step function is smoothed when using $k(z)$ = constant as input guesses in the fitting process. Any prior knowledge of the form of the gradient as can be obtained by intensity normalization of multiple angle data or variation of the refractive index of the incident medium is a valuable aide in the improvement of input guesses and the subsequent gradient calculation.

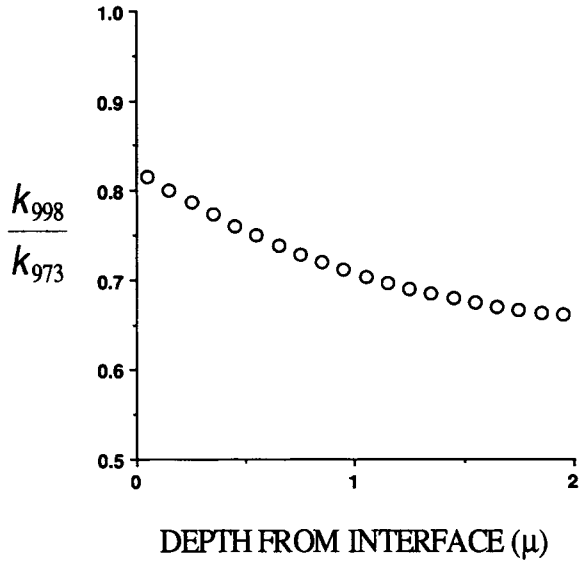

Figure 13 Isotropic equivalent absorbance ratio of 998 and 973 cm^{-1} bands vs. depth for uniaxially oriented isotactic polypropylene.

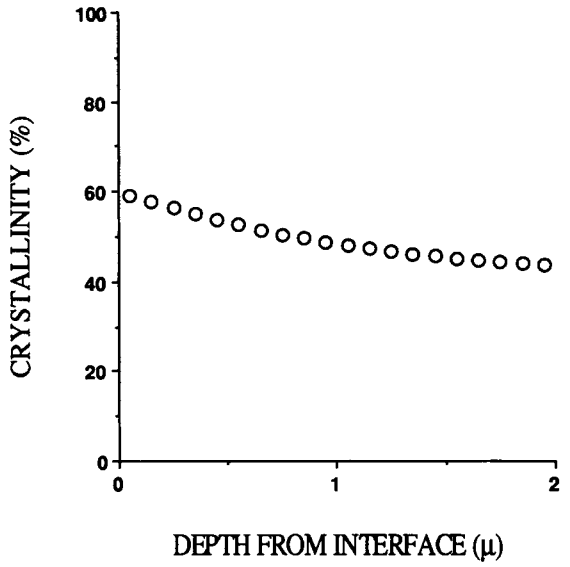

Figure 14 Calculated degree of crystallinity vs. depth for uniaxially oriented isotactic polypropylene.

Acknowledgment is made to the donors of the Petroleum Research Fund, administered by the ACS, for partial support of this research.

REFERENCES

1. K. G. Tingey and J. D. Andrade, *Langmuir,* **7,** 2471 (1991).
2. J. A. Gardella, *Appl. Surf. Sci.,* **31,** 72 (1988).
3. Q. S. Bhatia, D. H. Pan, and J. T. Koberstein, *Macromolecules,* **21,** 2166 (1988).
4. N. L. Franchina and T. J. McCarthy, *Macromolecules,* **24,** 3045 (1991).
5. W. M. Reichert, P. A. Suci, J. T. Ives, and J. D. Andrade, *Appl. Spectrosc.,* **41,** 503 (1987).
6. R. M. Dittmar, J. L. Chao, and R. A. Palmer, *Appl. Spectrosc.,* **45,** 1104 (1991).
7. D. R. Miller and P. W. Bohn, *Anal. Chem.,* **60,** 407 (1988).
8. M. W. Urban and J. L. Koenig, in *Vibrational Spectra and Structure 18 Applications of FT-IR Spectroscopy,* J. R. Durig, Ed., Elsevier, Amsterdam, 1990, Chap. 3.
9. R. Popli and A. M. Dwivedi, *J. Appl. Polym. Sci.,* **37,** 2469 (1989).
10. G. Zerbi, G. Gallino, N. Del Fanti, and L. Baini, *Polymer,* **30,** 2324 (1989).
11. L. J. Fina and G. C. Chen, *Vib. Spectrosc.,* **1,** 353 (1991).
12. L. J. Fina and G. C. Chen, *Ind. Eng. Chem. Res.,* **31,** 1659 (1992).

13. L. J. Fina, in *Structure-Property Relations in Polymers: Spectroscopy and Performance,* C. Claver and M. Urban, Eds., American Chemical Society, Washington, DC, to appear.
14. H. Ishida and R. Shick, *Polym. Prepr.,* **32**(3), 677 (1991).
15. M. Harada, T. Kitamori, N. Teramae, K. Hashimoto, S. Oda, and T. Sawada, *Appl. Spectrosc.,* **46,** 529 (1992).
16. A. E. Tshmel, V. I. Vettegren, and V. M. Zolotarev, *J. Macromol. Sci. Phys.,* **B21,** 243 (1982).
17. J. P. Hobbs, C. S. P. Sung, K. Krishnan, and S. Hill, *Macromolecules,* **16,** 193 (1983).
18. A. Pirnia and C. S. P. Sung, *Macromolecules,* **21,** 2699 (1988).
19. T. Hirschfeld, *Appl. Spectrosc.,* **31,** 289 (1977).
20. S. Teitler and B. W. Henvis, *J. Opt. Soc. Am.,* **60,** 830 (1970).
21. I. M. Minkov, *Opt. Spektrosk.,* **37,** 309 (1974).
22. A. N. Parikh and D. L. Allara, *J. Chem. Phys.,* **96,** 927 (1992).
23. P. A. Flournoy and W. J. Schaffers, *Spectrochim. Acta,* **22,** 5 (1966).
24. A. J. de Vries, *Pure Appl. Chem.,* **53,** 1011 (1981).
25. K. M. Brown and J. E. Dennis, *Numer. Math.,* **18,** 289 (1972).
26. B. Jasse and J. L. Koenig, *J. Macromol. Sci.-Rev. Macromol. Chem.,* **C17,** 61 (1979).
27. G. Zerbi and L. Piseri, *J. Chem. Phys.,* **49,** 3840 (1968).
28. S. Krimm, *Fortschr. Hochpolym. Forsch.,* **2,** 51 (1960).
29. H. Tadokoro, M. Ukita, M. Kobayashi, and S. Murahashi, *J. Polym. Sci.,* **B1,** 405 (1963).
30. Y. Kobayashi, S. Okajima, and A. Narita, *J. Appl. Polym. Sci.,* **11,** 2515 (1967).
31. R. J. Samuels, *Makromol. Chem. Suppl.* **4,** 241 (1981).
32. M. K. Gupta, D. J. Carlsson, and D. M. Wiles, *J. Polym. Sci. Polym. Phys.,* **22,** 1011 (1984).
33. F. M. Mirabella, *J. Polym. Sci. Polym. Phys.,* **23,** 861 (1985).
34. G. Bayer, W. Hoffmann, and H. W. Siesler, *Polymer,* **21,** 235 (1980).
35. R. G. Quynn, J. L. Riley, D. A. Young, and H. D. Noether, *J. Appl. Polym. Sci.,* **2,** 166 (1959).

Received May 2, 1992
Accepted June 30, 1992